JOURNAL OF MATERIALS SCIENCE 26 (1991) 2063–2070

Helium-induced weld cracking in austenitic and martensitic steels

H. T. LIN*, B. A. CHIN
Materials Engineering, Auburn University, AL 36849, USA

Helium was uniformly implanted into type 316 stainless steel and Sandvik HT-9 (12Cr–1MoVW) to levels of 0.18 to 256 and 0.3 to 1 a.p.p.m., respectively, using the "tritium trick" technique. Autogenous bead-on-plate, full penetration, welds were then produced under fully constrained conditions using the gas tungsten arc welding (GTAW) process. The control and hydrogen-charged plates of both alloys were sound and free of any weld defects. For the 316 stainless steel, catastrophic intergranular fracture occurred in the heat-affected zone (HAZ) of welds with helium levels ≥ 2.5 a.p.p.m. In addition to the HAZ cracking, brittle fracture along the centreline of the fusion zone was also observed for the welds containing greater than 100 a.p.p.m. He. For HT-9, intergranular cracking occurred in the HAZ along prior-austenite grain boundaries of welds containing 1 a.p.p.m. He. Electron microscopy observations showed that the cracking in the HAZ originated from the growth and coalescence of grain-boundary helium bubbles and that the fusion-zone cracking resulted from the growth of helium bubbles at dendrite boundaries. The bubble growth kinetics in the HAZ is dominated by stress-induced diffusion of vacancies into bubbles. Results of this study indicate that the use of conventional GTAW techniques to repair irradiation-degraded materials containing even small amounts of helium may be difficult.

1. Introduction

The bombardment of structural components of fission nuclear reactors with high-energy neutrons will produce significant physical damage to materials by atomic displacement and result in the production of helium by accompanied (n, α) reactions [1–4]. As a consequence, degradation of mechanical properties will occur. Because the neutron spectrum of the envisioned fusion reactors contains a higher portion of even more energetic neutrons, it is anticipated that the degradation phenomena will be more severe. Such deterioration of structural components plays a decisive role in limiting the useful lifetime of nuclear reactors. To achieve economic operation of both fission and fusion power reactors, it is reasonable to assume that repair and replacement of these degraded components will be required. Such repair processes will require the use of conventional welding techniques.

Apart from the high radioactive hazards, the major effect that will be encountered during the welding of irradiated materials is the entrapped helium produced by transmutation reactions in the materials. The degradation of the high-temperature mechanical properties of neutron-irradiated materials due to the presence of grain-boundary (GB) helium bubbles has been known for several decades [3]. Because of the very low solubility of helium in metals it has a strong tendency to precipitate out into bubbles. The formation of GB helium bubbles will lead to dramatic changes in macroscopic properties, including high-temperature embrittlement. These bubbles will grow rapidly under the influence of high temperature and stress. As these bubbles coalesce along the grain boundaries, intergranular fracture occurs prematurely. Because the welding process produces internal tensile stresses and high temperatures, the growth of entrapped helium bubbles may be strongly enhanced, speeding the degradation of properties.

To date only a few studies involving the welding of irradiated materials have been reported [5–7]. Unfortunately, none of these have provided a systematic characterization of the observed weld defects and conclusive results. Accordingly, a better understanding of the relationship between helium and weld cracking has not been pursued. This research was carried out to provide further insight into the effect of helium on the weldability of materials. Furthermore, the kinetics of processes which dictate GB bubble growth during the welding of helium-containing materials is elucidated. To reduce the radiological hazards and the difficulties involved with remote hot-cell operations, helium was introduced into the test materials through tritium decay (the "tritium trick" technique) prior to welding. This approach may provide a feasible way to evaluate the principal effect of helium on the joining of irradiated materials. This technique assumes that dislocation loops, networks and voids induced by

* *Present address*: Metals and Ceramics Division, Oak Ridge National Laboratory, Oak Ridge, TN 37831-6068, USA.

0022–2461/91 $03.00 + .12

neutron irradiation play a minor role during the welding of irradiated materials.

2. Experimental procedure

In this study, austenitic type 316 stainless steel (heat 8 092 297) was investigated as a primary alloy, and Sandvik HT-9 (heat 9607R2) as a secondary alloy. These two alloys have been studied extensively in the US Fast Breeder Reactor Program [8]. Detailed chemical compositions for both alloys can be found in [8]. Sandvik HT-9 (12Cr–1MoVW) was studied to determine the applicability of the type 316 stainless steel results to other classes of steel. The 0.76 mm thick sheets of type 316 stainless steel were solution-annealed at 1050 °C for 1 h, while those for HT-9 were solution-annealed at 1050 °C for 0.5 h followed by a tempering treatment at 750 °C for 1 h.

The "tritium trick" technique [9] was employed to implant helium into the test materials. In this technique the materials were exposed to high tritium gas pressure at elevated temperatures. The dissolved tritium is then allowed to decay to form helium by the reaction $^3H \rightarrow {}^3He + \beta^-$ with a half-life of tritium of 12.3 years. All specimens were charged at 300 °C for 30 days under tritium pressures ranging from 0.07 to 125 MPa. At the end of this charging period, the exposed materials were removed from the high-pressure charging vessel and held at 400 °C at 10^{-3} Pa in order to remove the residual tritium and to stop further generation of helium. Thus by varying the tritium charging pressure, a wide range of helium levels was generated. Table I lists the detailed charging condition for both alloys. Following the charging process, the helium concentration was quantitatively measured using vacuum fusion mass spectroscopy [10]. To demonstrate that weld defects which occurred during welding arose only from the helium rather than residual tritium, type 316 stainless steel was also charged with hydrogen under the same charging conditions as for the higher helium content specimens. The hydrogen-charged materials were then subjected to the same welding procedures as applied to type 316 stainless steel and examined for hydrogen-induced weld defects.

Autogenous bead-on-plate welds were made on control, hydrogen-charged and helium-doped materials using the gas tungsten arc welding (GTAW) process. Welding was performed in a high-velocity airhood with air flow rate of 1.5 m s^{-1}, as shown in Fig. 1. The motion of the welding torch was controlled by a Unislide stepping motor translator. For type 316 stainless steel, full-penetration welds were produced in the 0.76 mm thick plate at 10 V d.c., 24 A at a travel speed of 3.6 mm s^{-1} (8.5 in min^{-1}) under a protective argon atmosphere, trapped by a plastic chamber. Run-off tabs were used to produce a uniform weld bead over the entire length of the weld plate. The plates were laterally constrained with stainless steel bars to simulate the structural restraint experienced by actual irradiated components during weld repair. To protect the back side of the weld from oxidation, a backing argon gas was used. A gas flow of 1.57×10^{-4} m^3 s^{-1} (20 ft^3 h^{-1}) argon was used. HT-9 plates were welded at 10 V d.c., 28 A at a travel speed of 3.6 mm s^{-1} (8.5 in min^{-1}) under the same constraint conditions as type 316 stainless steel. The as-tempered HT-9 was not preheated prior to welding. The welding process of type 316 stainless steel was videotaped to provide a permanent record of real-time and macroscopic response (cracking) of the materials during welding.

Following welding, the as-welded plates were examined in detail using a scanning electron microscope (SEM). The weld microstructures were also examined by preparing metallographic sections transverse to the welding direction. The sections of type 316 stainless steel were electrolytically etched in a solution of 40% HNO_3–60% H_2O and those of HT-9 were etched chemically in a solution of 1% HF, 9% HNO_3 and 90% H_2O. The helium bubble morphology in the heat-affected zone (HAZ) was examined using a Philips CM-12 transmission electron microscope (TEM) operated at 120 keV. Thin foils for TEM work were prepared from 3 mm diameter discs cut from the 0.76 mm plate. The discs were polished on 600 grit paper to a thickness of 0.25 mm and were subsequently electropolished in a Struers Tenupol using a 12.5% sulphuric acid in methanol solution at − 15 °C, 120 mA and 20 V d.c.

TABLE I The helium-doping conditions of type 316 stainless steel and HT-9 at 300 °C

Material	He level (a.p.p.m.)	Pressure (MPa)	Time (h)
316 SS[a]	0.18	0.07	720
	2.50	1.70	720
	27.00	38.00	720
	105.00	125.00	720
	256.00[b]	125.00	720
	Hydrogen	125.00	500
HT-9[a]	0.30	1.70	720
	1.00	38.00	720

[a] Materials were degassed at 10^{-3} Pa and 400 °C for 118 h.
[b] Materials were stored at − 40 °C for 6 months after the "tritium trick" technique.

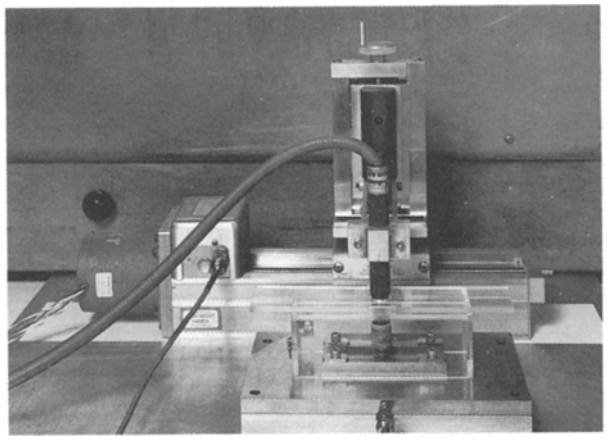

Figure 1 Experimental welding station located in a high-velocity airhood.

3. Results

3.1. Austenitic stainless steel welds

Results of SEM examination and metallography of type 316 stainless steel revealed that helium-free welds (control and hydrogen-charged) and welds with the lowest helium content (0.18 a.p.p.m.) were sound and free of weld defects. However, specimens with helium contents greater than 0.18 a.p.p.m. all showed significant degradation in weldability. Fig. 2 shows the representative features of as-welded type 316 stainless steel with 2.5 a.p.p.m. He. Severe continuous, through-thickness cracking in the HAZ was consistently observed in all of the as-welded plates (five out of five), as shown in Fig. 2a. Typically, HAZ cracking occurred one to three grain diameters from the fusion boundary, and was fully intergranular in nature (Fig. 2b). Because no external stresses were pre-applied, the cracking, in all cases, resulted from the generation of tensile thermal stresses as the constrained plates cooled after the passing of the welding torch. At higher magnification, the grain facets were observed to be decorated with a uniform distribution of dimples attributed to coalesced helium bubbles (Fig. 2c). The average dimple size was approximately 1 μm and was independent of helium concentration. Incipient cracking, arising from coalescence of cavities, was also observed along the grain-boundary intersections. In addition, the shear ligaments separating the dimples had been rounded by surface diffusion, indicating that the cracking occurred at high temperatures early in the weld-cooling cycle. This is consistent with videotape recordings that HAZ cracking occurred approximately 1 s after the resolidification of the molten weld pool. According to the measured thermal history in the HAZ, the temperature at which fracture occurred was about 1150 °C [11].

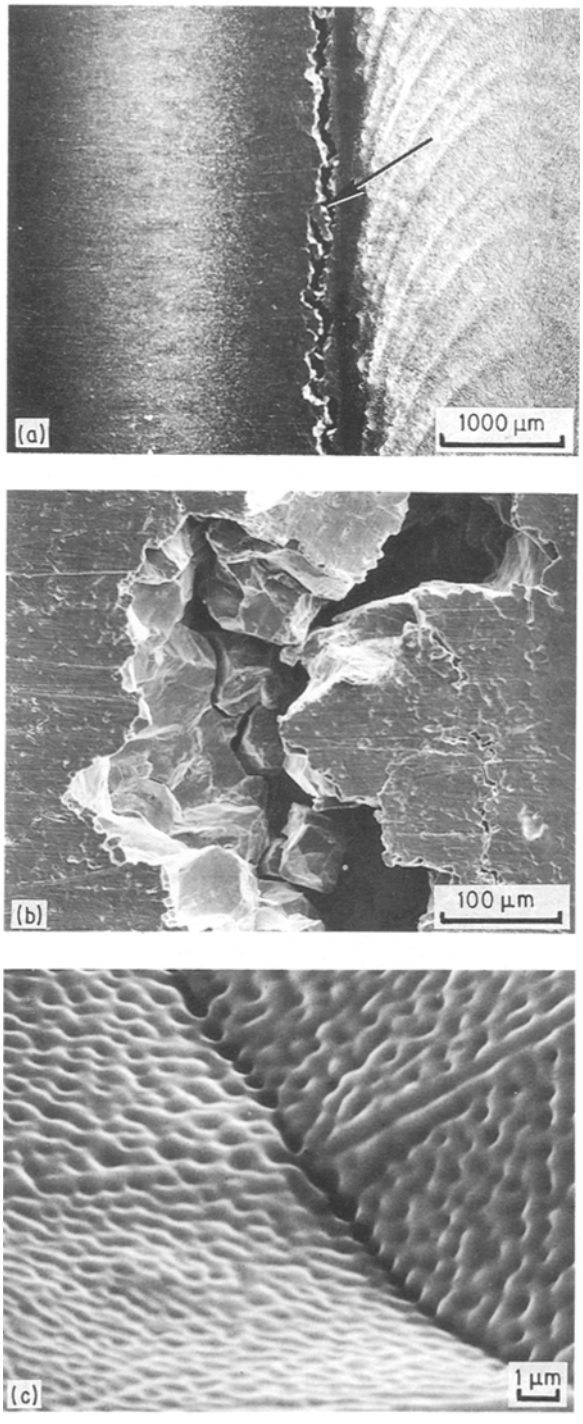

Figure 2 Morphological features of as-welded 316 stainless steel with 2.5 a.p.p.m. He. (a) Photomacrograph of heat-affected zone showing intergranular cracking, (b) scanning electron micrograph of detailed intergranular fracture, (c) scanning electron micrograph of grain-boundary facets decorated with a uniform distribution of dimples.

The microscopic weld features for higher helium level material (105 a.p.p.m.) is shown in Fig. 3. All of the welded plates (seven out of seven) revealed catastrophic HAZ cracking similar to that described for the lower helium-containing materials (2.5 and 27 a.p.p.m.). As in the previous case, the HAZ cracking was fully intergranular in nature and occurred within one to three grain diameters from the fusion boundary. In addition to HAZ cracking, centreline cracking in the fusion zone also occurred in more than 60% of the welded plates (Fig. 3a). SEM analysis of the fusion zone centreline cracking indicated that the brittle fracture proceeded along dendrite boundaries during weld metal resolidification. Large spherical pores resulting from the growth of entrapped helium bubbles were also observed on the fracture surface.

Fig. 4 shows the optical microstructure of the welds from a section taken transverse to the welding direction for the control and specimens containing 0.18, 2.5 and 105 a.p.p.m. He. Generally, the microstructure of the fusion zone was primary austenite with ferrite precipitation in the dendrite boundaries. Small amounts of ferrite precipitation were also observed surrounding the grain boundaries at the fusion–HAZ boundary. In the helium-bearing specimens, spherical pores decorating the dendrite boundaries were observed. Based on the comparison of the observed microstructures in the helium-free and helium-containing materials, it was concluded that the visible pores in the fusion zone are helium bubbles. In addition, it is clear that the density and size of porosity in the helium-doped welds increase with increasing helium concentrations.

Results of metallography indicated that both control and hydrogen-charged welds were found to be uncracked and free of any damage. Therefore, it is clear that the degradation in weldability, occurrence of fusion zone as well as HAZ cracking, is entirely

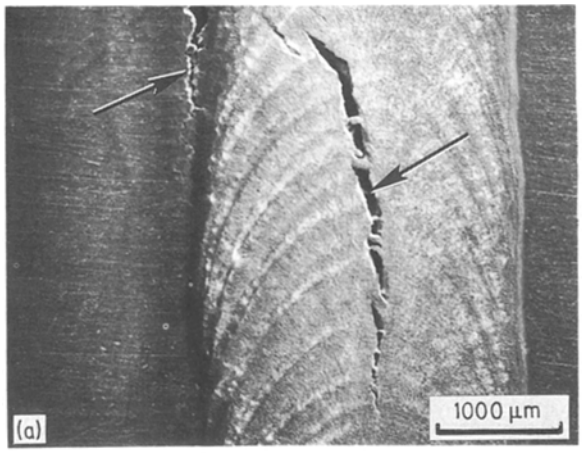

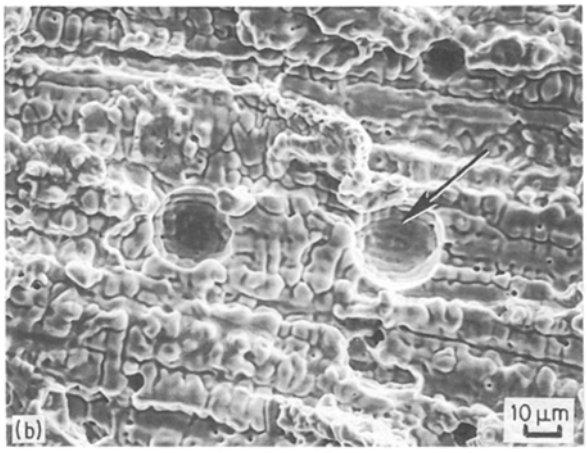

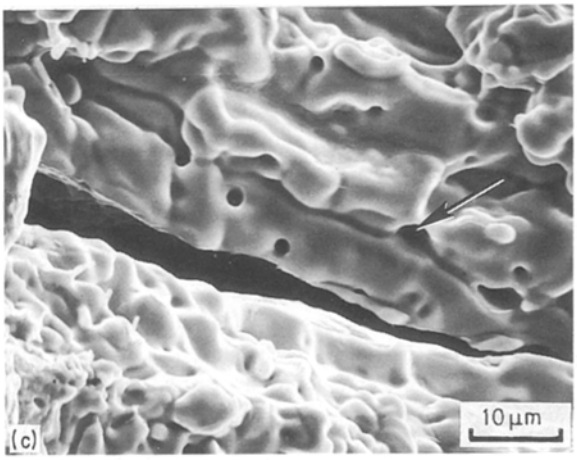

Figure 3 Morphological features of as-welded 316 stainless steel with 105 a.p.p.m. He. (a) Photomacrograph of brittle fracture in fusion and heat-affected zones, (b) scanning electron micrograph showing brittle failure of the fusion zone, (c) scanning electron micrograph showing fusion zone fracture proceeds along an inter-dendritic path and helium bubbles at dendrite boundaries.

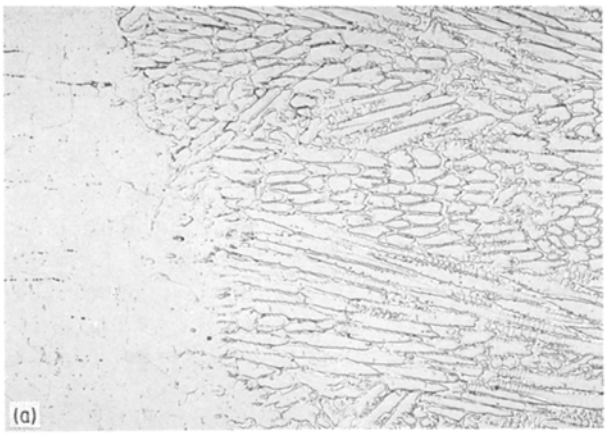

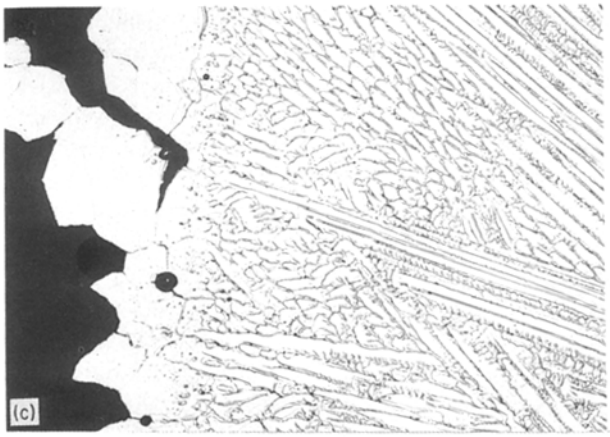

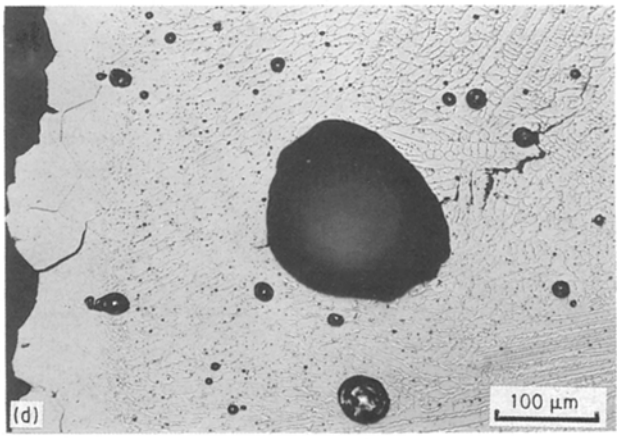

Figure 4 Optical metallography of type 316 stainless steel welds taken transverse to the welding direction. (a) Control material, (b) 0.18 a.p.p.m., (c) 2.5 a.p.p.m., (d) 105 a.p.p.m. Note failure occurred in the heat-affected zone.

related to the entrapped helium rather than to the residual hydrogen or tritium. Also, the metallography analysis revealed that the intergranular cracking occured not at the fusion zone–HAZ boundary but in the HAZ. This suggests that peak temperature alone is not the main driving force for weld cracking. Rather, a critical combination of high temperature and high stress must be the key factor in controlling the bubble growth and crack formation. An annealing study at temperatures up to 1300 °C for 1 h on unstressed TEM discs and tensile specimens containing 256 a.p.p.m. He was conducted to verify this hypothesis [11]. None of the annealed specimens displayed any sign of cracking after the high-temperature ageing. The 1300 °C aged specimens showed much smaller GB helium bubbles (0.1 μm) than those observed on the HAZ cracking surfaces (1 μm). Additionally, all of the aged specimens tested at room temperature still showed good ductility (> 35% total elongation). These results support the hypothesis that high peak temperature alone is not sufficient to induce HAZ cracking. Because no external loads were applied prior to welding, the cracking resulted from the generation of tensile thermal stresses as the laterally constrained plates cooled after the passing of the torch.

Following welding, the helium bubble morphology in the HAZ was studied in detail using transmission electron microscopy. The TEM discs were sectioned from the uncracked regions. In the HAZ of the lowest helium containing materials (0.18 a.p.p.m.), which did not show any weld defects, GB helium bubbles were rarely observed. On the contrary, most of the grain boundaries for materials containing 2.5 a.p.p.m. He and above, contained bubbles and were preferentially perforated during the specimen thinning process. Fig. 5 shows the typical helium bubble morphology in the HAZ of welded helium-doped specimens (256 a.p.p.m.). This preferential perforation was caused by the presence of very large helium bubbles located along the grain boundaries (Fig. 5a). The perforations were similar in size to the observed dimples on the HAZ fracture surface (Fig. 2c). This observation further confirms that dimples on the HAZ cracking surfaces are helium bubbles, indicating that the grain boundaries in the discs were very near the final stage of cracking. Grain-boundary helium bubbles in the HAZ were much larger than those observed in the as-implanted condition. The increase in bubble size resulted from their growth which was enhanced by the actions of temperature and thermally induced stress. The density and size of helium bubbles in the HAZ also varied from boundary to boundary. The differences were apparently due to the variation in the orientation of grain boundaries with respect to the shrinkage tensile stress and to the thermal history experienced by each individual grain boundary. The boundaries which experienced the most critical combination of high temperature and stress would be expected to have the largest helium bubbles, as observed in the HAZ fracture surface.

3.2. Martensitic steel welds

The postweld examination of HT-9 plates indicated that no weld defects were found in the control specimens and in plates with the lowest helium content (0.18 a.p.p.m.). However, the welds containing 1 a.p.p.m. He showed discontinuous micro-cracking in the HAZ within several grains from the fusion boundary. The observed cracking was limited to the beginning region of the weld. Observations showed that weld cracking along the prior-austenite grain boundaries was fully intergranular in nature, as shown in Fig. 6a. At higher magnification the grain facets were observed to be decorated with a uniform distribution of dimples (Fig. 6b). The shear ligaments have been rounded by surface diffusion, indicating that cracking occurred at high temperatures. As stated for type 316 stainless steel, the cracking resulted from shrinkage stresses as the constrained plates cooled after welding. Again, the HAZ cracking originated from the growth and coalescence of GB helium bubbles.

4. Discussion

4.1. Heat-affected zone

As both the control and hydrogen-charged specimens were welded successfully, it is apparent that the loss of

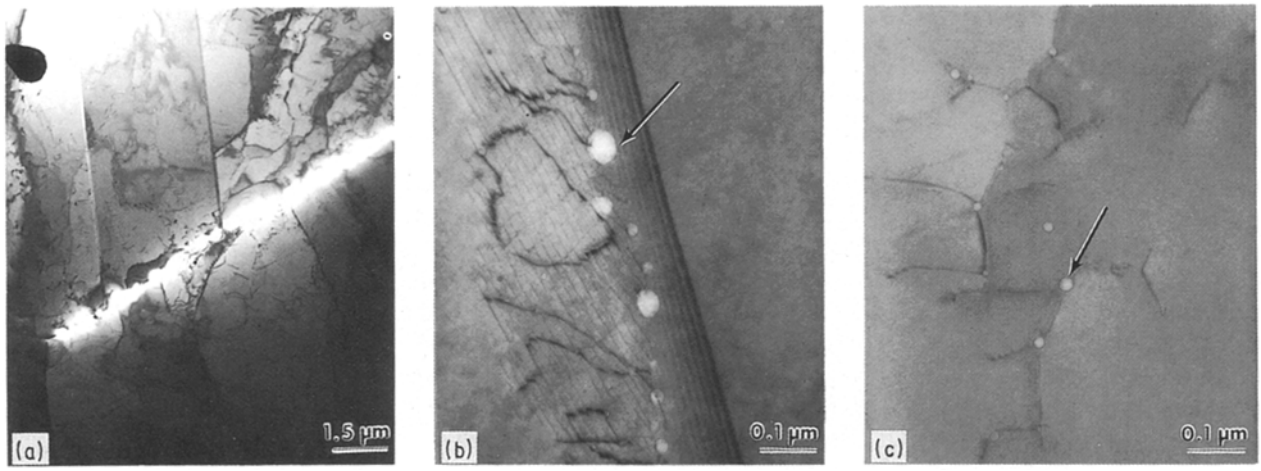

Figure 5 Transmission electron micrograph of the heat-affected zone of type 316 stainless steel with 256 a.p.p.m. He. (a) Perforated grain boundary, (b) grain-boundary helium bubbles, (c) matrix helium bubbles attached to dislocations.

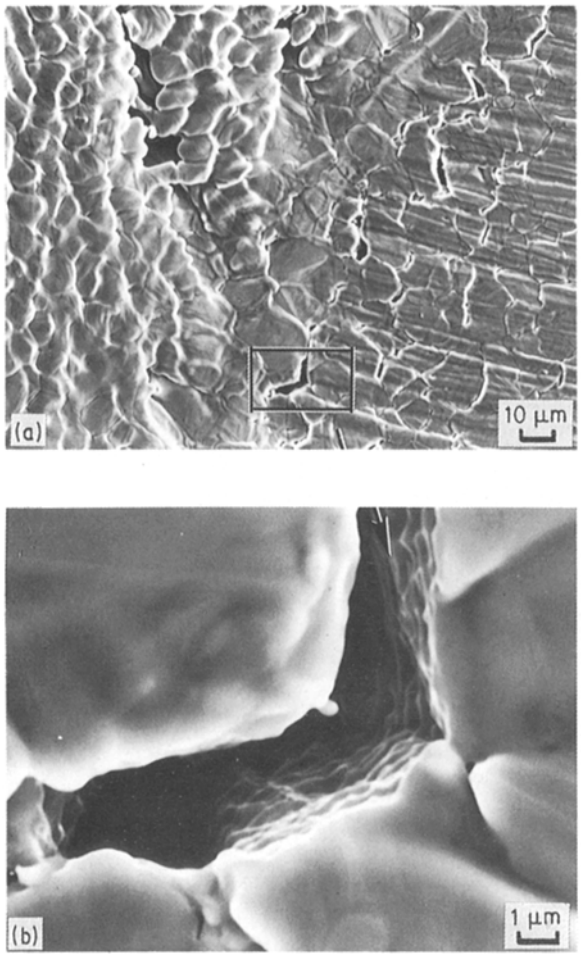

Figure 6 Morphological features of as-welded Sandvik HT-9 containing 1 a.p.p.m. He. (a) Intergranular fracture along prior-austenite grain boundaries, (b) grain-boundary facets decorated with a uniform distribution of dimples.

alloy weldability in both type 316 stainless steel and HT-9 is due to the entrapped helium rather than any remaining tritium. The scanning electron micrographs for both alloys revealed that intergranular cracking occurred in the HAZ. Also, the grain facets were observed to be decorated with a uniform distribution of dimples attributed to helium bubbles. The TEM microstructure of type 316 stainless steel showed grain boundaries perforated by the presence of helium bubbles. These observations demonstrate that brittle fracture observed in the HAZ resulted from the growth and coalescence of GB helium bubbles under the influences of high temperature and shrinkage thermal stress. Nevertheless, the lowest helium content materials, 0.18 a.p.p.m. type 316 stainless steel and 0.3 a.p.p.m. HT-9, were welded successfully. This suggests that a threshold level (between 0.18 and 1 a.p.p.m.) of helium exists below which materials may be welded successfully using conventional GTAW processes.

The growth of GB helium bubbles is favoured by conditions that promote high temperature and stress. In the case of welding, the high temperatures originate from the welding arc, and tensile stresses are generated by the cooling of the constrained plates. The precipitated helium bubbles, which nucleated and formed during the charging period, grew under the actions of high temperature and stress until the reduced contact areas of the grain boundaries could no longer bear the shrinkage-imposed tensile stress, leading to final brittle rupture. A model describing the GB helium bubble growth leading to brittle fracture in the HAZ has been proposed [11]. The growth kinetics of GB helium bubbles in the HAZ can be divided into three sequential time regimes, as shown in Fig. 7. This division is made to recognize the different stress states and temperatures that a fixed point in the HAZ experiences as the welding arc passes. Regime I is the heat-up period before the temperature reaches the melting point. During this regime, compressive stress is present. Regime II is chosen as the time interval during which the molten pool is present resulting in a stress-free state at the pool surface in the transverse direction. Regime III occurs after the molten pool has begun to re-solidify and internal tensile shrinkage stresses are generated in the constrained plate.

During the first regime, compressive stresses generated by the thermal expansion of the material will retard bubble growth at grain boundaries normal to the compressive stresses. Hence, GB bubble growth takes place mainly during time regimes II and III. During Regime II, the growth of GB helium bubbles is hypothesized to be primarily governed by the absorption of vacancies into bubbles. This process is particularly favoured at temperatures close to the melting point where there is a high vacancy concentration available. Because during time regime II the HAZ is in a stress-free state, the bubble growth is driven by the helium gas overpressure in the bubbles. The bubble growth rate in regime II can be expressed by

$$dr/dt = \delta\Omega D_{gb} C_v^e / 2r^2 \quad (1)$$

where δ is grain-boundary thickness available for diffusion, Ω is atomic volume, D_{gb} is the self-diffusion coefficient in the grain boundary, C_v^e is thermal equilibrium vacancy concentration and r is the bubble radius. Using Equation 1 the size of GB helium bubbles in the HAZ at the end of regime II can be calculated. For a position one to three grains from the fusion boundary, the bubble size is approximately 50 nm after regime II. This result is obtained by specifying $\delta = 0.4$ nm, $\Omega = 10^{-29}\,m^3$, $D_{gb} = 1.2 \times 10^{-9}\,m^2\,s^{-1}$ [12], $C_v^e = 2.1 \times 10^{-24}\,1\,m^{-3}$ and $\Delta t = 1.7$ s (time spent in regime II).

Once the materials in the weld pool start to solidify (regime III), the kinetics of GB helium bubble growth in the HAZ is controlled by the internal tensile stress developed during cooling. The laterally imposed external constraints will further enhance the magnitude of internal tensile stresses generated. During regime III, the growth of GB helium bubbles is dominated by the stress-enhanced diffusive cavity growth which has been studied extensively for the last three decades [13–19]. The growth rate of GB cavities during regime III can be obtained from [13]

$$dr/dt = 2\pi\delta\Omega D_{gb}\sigma/arkT \quad (2)$$

where a is the centre to centre cavity spacing, σ is the shrinkage tensile stress (transverse to the welding direction) normal to the grain boundary, and kT has

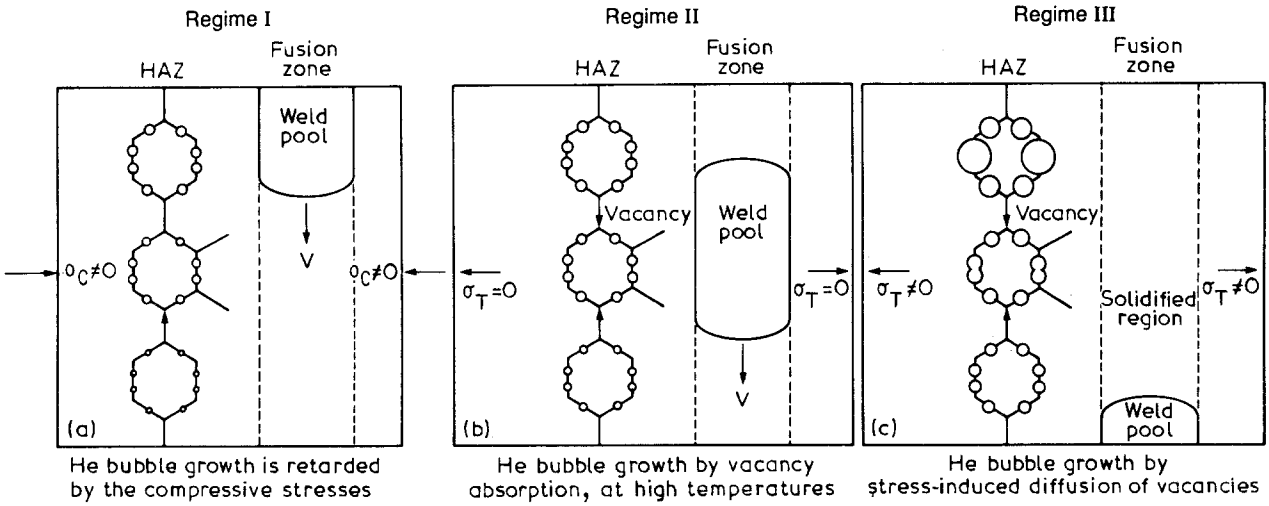

Figure 7 Schematic diagram showing the growth kinetics of grain-boundary helium bubbles in the heat-affected zone during welding. (a) Time regime I, heat-up period; (b) time regime II, molten pool present and stress free state; (c) time regime III, cooling period of resolidified metal and shrinkage tensile stresses present.

its usual meaning. The bubble size can be obtained by integration of Equation 2 if D_{gb}, σ and T as functions of time are known. Generally, these relationships can be obtained theoretically and/or experimentally as explicit functions of time. During cooling, temperature in the HAZ as a function of time was experimentally determined and can be expressed empirically as [11]

$$T(t) = 20 + 1906 \exp\{-668388/[t(T_p - 20)^2]\}/t^{1/2} \quad (3)$$

where T is in °C and t in s. Consequently, D_{gb} as a function of time can be expressed by [12]

$$D_{gb} = 2 \exp[-1.65\,\text{eV}/kT(t)]\,\text{cm}^2\,\text{s}^{-1} \quad (4)$$

For the present case the transverse shrinkage tensile stresses (σ) resulting from the cooling of the weld as a function of time are difficult to describe explicitly. From the elasticity theory, the thermal stress can be related to the Young's modulus (E) and the thermal expansion coefficient (α) which are functions of temperature and therefore functions of time. The thermal stress present at any instant is given by

$$\sigma(t) = E(t)\alpha(t)\Delta T \quad (5)$$

An approximate relationship between thermal stress and time can then be obtained. Consequently, the bubble size in the HAZ during regime III can be estimated by integrating Equation 2. The model predicts that bubbles in grain boundaries one to three grain diameters from the fusion line should reach approximately 0.85 μm diameter, 1 s after the passing of the torch. The prediction compares favourably with the experimentally measured dimple size (1 μm) on the HAZ fracture surface at the onset of cracking (1 s). Although it is likely that internal microcracks initiated earlier than the onset of the evident HAZ cracking as measured from the videotape, reasonable consistency between the predicted and measured bubble size supports the validity of the proposed model.

The model of GB bubble growth in the HAZ developed for type 316 stainless steel can also be applied to the case of HT-9, although HT-9 has a radically different microstructure. This is due to the fact that HT-9 undergoes a phase transformation at about 850 °C from the ferrite structure (body-centred cubic) to austenite (face-centred cubic) [20]. In the region 850–1350 °C (melting point), HT-9 is anticipated to behave similarly to austenitic stainless steel. The only difference in predictions would be due to the differences in the specific diffusivities in this temperature range. Based upon similar diffusivities, it is anticipated that the kinetics of GB bubble growth in the HAZ of HT-9 are similar to those in type 316 stainless steel.

4.2. Fusion zone

Fractography of the fusion zone of type 316 stainless steel with helium levels ≥ 105 a.p.p.m. revealed that brittle fracture proceeded along the dendrite boundaries (Fig. 3c). The SEM observations suggest that brittle fracture is caused by the growth of helium bubbles in the dendrite boundaries. As solidification proceeds, helium is rejected by the growing dendrites because of the low solubility of helium in the metal and is trapped between dendrites in regions which are the last to solidify. These bubbles coalesce into microcracks. Tensile shrinkage stresses, which are the highest at the fusion centreline [21], cause these cracks to propagate leading to brittle rupture along the centre of the fusion zone.

In summary, this study shows that brittle fracture can occur in both the fusion zone and HAZ due to the growth and coalescence of helium bubbles at dendrite boundaries and grain boundaries, respectively. A critical combination of high temperature and high tensile stress is a key factor in controlling the growth of GB helium bubbles in the HAZ. This study suggests that repair of neutron degraded components containing even small amounts of helium by conventional GTAW processes may be difficult.

5. Conclusions

This study of helium effects on the subsequent weldability of austenitic and ferritic steels leads to the following conclusions:

1. Catastrophic intergranular HAZ cracking occurred during cooling of GTA-welded type 316 stainless steel and HT-9 with helium levels equal to or greater than about 2.5 and 1 a.p.p.m., respectively.

2. Brittle fracture in the HAZ of both alloys originates from the growth and coalescence of GB helium bubbles, while brittle fracture in the fusion zone of type 316 stainless steel results from the growth of helium bubbles at dendrite boundaries.

3. High peak temperatures alone are not sufficient to induce heat-affected zone cracking. Both high temperatures and high stresses induced by the imposed constraints are necessary.

4. Repair of irradiated structural components containing helium levels greater than about 1 a.p.p.m. by conventional GTA welding processes may be difficult.

Acknowledgements

The authors thank R. H. Zee, Auburn University, R. L. Klueh and J. H. Schneibel, Oak Ridge National Laboratory, for reviewing the manuscript. The technical contribution from J. W. Jones is much appreciated. This research was sponsored by the Office of Fusion Energy, US Department of Energy under Contract DE-AC05-84OR21400 with Martin Marietta Energy Systems, Inc., Grant DEFG0585ER52139C with Auburn University, and by the Division of Materials Sciences, US Department of Energy under the SHaRE program (Contract DE-AC05-76OR00033) with Oak Ridge Associated Universities.

References

1. H. S. ROSENBAUM, "Treatise on Materials Science and Technology", Vol. 7 (Academic Press, New York, 1975).
2. J. O. STIEGLER and L. K. MANSUR, *Ann. Rev. Mater. Sci.* **9** (1979) 405.
3. R. S. BARNES, *Nature* **206** (1965) 1307.
4. D. R. HARRIES, *J. Nucl. Mater.* **82** (1979) 635.
5. M. M. HALL Jr, A. G. HINS, J. R. SUMMERS and D. E. WALKER, "Weldment: Physical Metallurgy and Failure Phenomena, Proceedings of the Fifth Bolton Landing Conference" (General Electric Co, Schenectady, New York, 1978) p. 365.
6. S. D. ATKIN, ADIP Semiannual Progress Report (September 1981) p. 110.
7. W. R. KANNE, C. L. ANGERMAN and B. J. EBERHARD, DP-1470 (E.I. du Pont de Nemours, Savannah River Laboratory, Aiken, SC, 1987).
8. B. A. CHIN, R. J. NEUHOLD and J. L. STRAALSUND, *Nucl. Technol.* **57** (1982) 426.
9. Annual Books and ASTM Standards, "Standard Guide for Simulation of Helium Effects in Irradiated Materials", Vol. 12.02, E492-83 (American Society for Testing and Materials, Philadelphia, PA) pp. 808–11.
10. B. M. OLIVER, J. G. BRADLEY and H. IV. FARRAR, *Geochim Cosmochim. Acta* **48** (1984) 1625.
11. H. T. LIN, PhD dissertation, Auburn University (1989).
12. D. W. JAMES and G. M. LEAK, *Phil. Mag.* **12** (1965) 491.
13. D. HULL and D. RIMMER, *ibid.* **4** (1959) 673.
14. M. V. SPEIGHT and J. E. HARRIES, *Metal Sci. J.* **1** (1967) 83.
15. J. WEERTMAN, *Scripta Metall.* **7** (1973) 1129.
16. M. V. SPEIGHT and W. BEERE, *Metal Sci. J.* **9** (1975) 190.
17. R. RAJ and M. F. ASHBY, *Acta Metall.* **23** (1975) 653.
18. H. TRINKAUS, *Ber. Bunsenges. Phys. Chem.* **82** (1978) 249.
19. H. RIEDEL, "Fracture at High Temperature" (Springer-Verlag, New York, 1987).
20. R. L. RICKETT, W. F. WHITE, C. S. WALTON and J. C. BUTLER, *Trans. ASM* **44** (1952) 138.
21. K. MASUBUCHI, "Analysis of Welded Structures" (Pergamon Press, New York, 1980) p. 189.

Received 30 October 1989
and accepted 6 June 1990